Paleoproterozoic oxygenated oceans following the Lomagundi-Jatuli Event

Kaarel Mänd[a, b], Stefan V. Lalonde[c], Leslie J. Robbins[d], Marie Thoby[c], Kärt Paiste[e], Timmu Kreitsmann[b], Päärn Paiste[b], Christopher T. Reinhard[f, g], Alexander E. Romashkin[h], Noah J. Planavsky[d, g], Kalle Kirsimäe[b], Aivo Lepland[b, e, i], Kurt O. Konhauser[a]

[a]Department of Earth & Atmospheric Sciences, University of Alberta, Edmonton, AB T6G 2E3, Canada.

[b]Department of Geology, University of Tartu, Ravila 14A, 50411 Tartu, Estonia.

[c]CNRS–UMR6538 Laboratoire Géosciences Océan, European Institute for Marine Studies, UBO, 29280 Plouzané, France.

[d]Department of Geology & Geophysics, Yale University, New Haven, CT 06511, USA.

[e]CAGE—Centre for Arctic Gas Hydrate, Environment and Climate, Department of Geosciences, UiT The Arctic University of Norway, 9037 Tromsø, Norway.

[f]School of Earth and Atmospheric Sciences, Georgia Tech, Atlanta, GA 30332, USA.

[g]NASA Astrobiology Institute Alternative Earths Team, University of California, Riverside, CA 9252, USA.

[h]Institute of Geology, Karelian Science Centre, Pushkinskaya 11, 185610 Petrozavodsk, Russia.

[i]Geological Survey of Norway (NGU), 7491 Trondheim, Norway.

The approximately 2220–2060 million years old Lomagundi-Jatuli Event was the longest positive carbon isotope excursion in Earth history and is traditionally interpreted to reflect increased organic carbon burial and a transient rise in atmospheric O_2. However, it is widely held that O_2 levels collapsed for more than a billion years following this. Here we show that black shales postdating the Lomagundi-Jatuli Event from the approximately 2000 million years old Zaonega Formation contain the highest redox-sensitive trace metal concentrations reported in sediments deposited before the Neoproterozoic (maximum concentrations of Mo = 1009 µg g^{-1}, U = 238 µg g^{-1}, Re = 516 ng g^{-1}). This unit also contains the most positive shale U isotope values measured to date (maximum $\delta^{238}U$ = 0.79‰), providing novel evidence that there was a transition to modern-like biogeochemical cycling during the Paleoproterozoic. Although these records do not preclude a return to anoxia during the Paleoproterozoic, they uniquely suggest that the oceans remained well-oxygenated millions of years after the termination of the Lomagundi-Jatuli Event.

The Paleoproterozoic era (2500–1600 Ma) witnessed the longest positive carbon isotope ($\delta^{13}C_{carb}$) excursion in Earth's history, recorded in marine carbonates deposited worldwide between ~2220–2060 Ma—the Lomagundi-Jatuli Event (LJE)[1,2]. Marine carbonates are generally characterized by $\delta^{13}C_{carb}$ values that vary between −5‰ to 5‰ for most of Earth's history, whereas peak LJE $\delta^{13}C_{carb}$ values reach 10–15‰[1]. There is ongoing debate regarding the processes that led to the LJE. The standard and most commonly accepted interpretation invokes increased burial of ^{13}C-depleted organic carbon (C_{org}), leading to the ^{13}C-enrichment of the dissolved inorganic carbon pool and positive $\delta^{13}C_{carb}$[1,3]. This acceleration in C_{org} burial may have been the result of an increase in oxidative weathering and nutrient delivery to the oceans[3]. Using

a simple isotope mass balance, it has been estimated that between 5–9×10^{20} mol of C_{org} was buried over 100 Ma, corresponding to the release of O_2 equivalents representing 12–22 times the present O_2 atmospheric pool. An ensemble of evidence points to atmospheric O_2 accumulation during the LJE, including proxies indicating growth of the marine sulphate reservoir[4–6], elevated concentrations of redox sensitive elements (RSE)[7–10], and evidence for locally oxic conditions[3,11]. However, others have argued that the 'standard' interpretation of the LJE is difficult to reconcile with our understanding of the C and O cycles[12,13], and that there is a notable paucity of C_{org}-rich deposits at this time[14], the most basic tracer of enhanced organic carbon burial. Further, the carbon isotope dynamics during and after the positive excursion are currently debated, and there are multiple interpretations of the LJE positive $\delta^{13}C_{carb}$ values that do not invoke elevated rates of organic carbon burial and oxygen release[13,15]. Therefore, additional constraints on carbon and oxygen cycling are clearly needed to refine our view of this time interval.

The 'standard' interpretation suggests that oxygen release due to C_{org} burial must have significantly slowed down in the aftermath of the LJE. In order to test this, we present new redox tracer data from two correlative sections (OnZaP and OPH sections; see Methods) of the upper Zaonega Formation (ZF), a post-LJE mudstone-dolostone succession. We provide some of the most straightforward evidence for Proterozoic surface oxygenation. In fact, current redox proxy records are most consistent with increasing oxygenation in the aftermath of the LJE—forcing a re-evaluation of our basic view of this turbulent interval of Earth's history.

Age and geochemical signatures of the Zaonega Formation

According to the latest U-Pb age constraints on a tuff horizon within the lower ZF, the formation was deposited at ~1980 Ma, ~80 Myrs after the proposed termination of the LJE[16]. This age

model is consistent with $\delta^{13}C_{carb}$ stratigraphy. In the Onega Basin, $\delta^{13}C_{carb}$ values in the lowermost ZF and underlying Tulomozero Formation are characterized by typical LJE values of ≥8‰ [17], with $\delta^{13}C_{carb}$ in preserved carbonate strata returning to normal marine values of ~0‰ further upsection[18]. In the OPH core, the studied section occurs after several hundred meters of stratigraphy—including cumulatively ~210 meters of mudstone-dominated sediments—and contains carbonates bearing a normal marine (and therefore post-LJE) $\delta^{13}C_{carb}$ signal[18]. Assuming a reasonable range of deposition rates for the mudstones—e.g., 1–100 m Myr^{-1} (Ref. 19)—the studied section of the ZF was deposited millions of years after the termination of the LJE in the Onega Basin.

The section is rich in total organic carbon (TOC), with average values of 27.4±18.5 wt.% in mudstones of the OnZaP section, and 14.5±9.9 wt.% in OPH mudstones (Figure 1). These values are roughly comparable to the most organic-rich modern marine sediments (e.g., up to 21.3 wt.% on the Peru margin[20]). We focus specifically on molybdenum (Mo), uranium (U), and rhenium (Re) enrichments, as these metals have previously provided robust evidence for major shifts in Earth's redox state[8,10,21]. In the Zaonega mudstones Mo, U, and Re are significantly elevated relative to other Proterozoic black shales[8,10,21], averaging 130±142 µg g^{-1}, 19±15 µg g^{-1}, and 116±84 ng g^{-1}, respectively, in OnZaP mudstones. In the OPH section, Mo and U average 71±92 µg g^{-1} and 37±50 µg g^{-1}, whereas overall maximum Mo, U, and Re concentrations across both sites are 1009 µg g^{-1}, 238 µg g^{-1}, and 516 ng g^{-1}, respectively. In the OnZaP section, $\delta^{98/95}$Mo is on average 0.67±0.81‰, with a maximum of 1.49±0.14‰. Uranium isotope values in the OnZaP section range from −0.03 to 0.79‰, with an average of 0.47‰. The maximum value is the most ^{238}U-enriched shale measurement that has been reported to date[22,23].

The primary source of these RSE (in the rest of this manuscript, RSE refers specifically to Mo, U, and Re) to the oceans is the oxidative weathering of terrestrial RSE-bearing minerals (e.g., pyrite, uraninite), and subsequent riverine transport as aqueous oxyanions[24,25]. Hydrothermal inputs, while not fully constrained at present, are not expected to be a quantitatively significant source for any of these RSE[21,25]. The most important RSE sink is sequestration into marine sediments, which is influenced by the redox state of the depositional setting[24,26]. In oxic seawater, RSE are present as recalcitrant species that tend to accumulate in the water column[25,27], although Mo adsorbs to Mn(IV)-oxides under oxic conditions and can then be released in pore waters following the reductive dissolution of Mn(IV)-oxides in anoxic sediments[28]. In anoxic environments, the RSE are progressively converted into particle-reactive species resulting in efficient drawdown through authigenic sulphide precipitation or adsorption to organic matter[26,27]. With regards to Mo, it has been found that most efficient Mo sequestration takes place under euxinic waters with >11 µM of sulphide (HS^-)[29]. In a broad sense, the contrasting behaviour of these elements in oxic and anoxic conditions ensures that the drawdown and marine reservoir sizes are governed by global ocean redox—large RSE reservoirs develop in an oxic ocean, which leads to large local sedimentary RSE enrichments under anoxic conditions[10,21].

The U and Mo isotope systems, similar to RSE enrichments, respond to the global marine redox landscape. There is consensus that well-oxygenated oceans are characterized by high Mo and U isotope values[30,31]. It is, however, difficult to gauge when a sedimentary archive captures seawater U and Mo isotope values. For instance, seawater Mo isotope values are most likely to be captured in shales deposited in isolated basins with high HS- levels[32]. However, non-quantitative reduction of Mo in euxinic marine basins results in negative fractionation and shale $\delta^{98/95}$Mo values that are lower than seawater[30], and therefore, $\delta^{98/95}$Mo in euxinic shales is often

interpreted as a minimum estimate for seawater $\delta^{98/95}$Mo[11]. Uranium isotope values in shales will be closest to seawater values in oxic sediments and up to ~1‰ heavier than seawater in anoxic and high productivity settings[31] (see Supplementary Information for detailed discussion on Mo and U isotope values). Using this framework, our data points to well-oxygenated oceans with high rates of primary productivity during deposition of the Zaonega Formation.

Marine RSE inventory

RSE enrichments in the ZF far exceed anything known from pre-Neoproterozoic black shales (Figure 2). Similar values are found only in the Phanerozoic, where they have been taken as evidence for an expanded seawater RSE inventory, the direct result of pervasive ocean-atmosphere oxygenation[8,10,21]. We believe that the ZF, likewise, contains evidence of a large marine RSE inventory that strongly suggests a relatively oxidized ocean–atmosphere system with a robust terrestrial oxic RSE weathering flux, in which the drawdown of RSE was limited by the relative scarcity of anoxic conditions on the seafloor. Further, U and Re enrichments—which, unlike Mo, are also drawn down in ferruginous waters[33]—suggest that this was an episode of thorough water column oxygenation on continental shelves, rather than just a restriction of euxinic deposition, >1.4 Gyr before terminal oceanic oxygenation during the Neoproterozoic[34].

While low Mo in black shales could be explained by either a small marine Mo pool, basinal restriction leading to localized Mo depletion[28], or inefficient Mo scavenging under low HS^- conditions[29], there are limited ways to explain elevated RSE concentrations in black shales of the ZF (i.e., up to several hundreds of μg g^{-1} of Mo throughout the >160 km-wide basin). One possibility is anomalously low sedimentation rates, which have previously been invoked to explain high TOC in U-rich black shales of the Miocene Monterey Formation, USA[35]. Although low

sedimentation rates may have played a role in concentrating TOC and RSE in the ZF, the magnitude of the RSE enrichment—consistent with Phanerozoic levels (Figure 2)—makes it unlikely sedimentation rate alone could account for it. A more plausible explanation is that the ZF was also a highly efficient RSE sink that had reliable access to a large oceanic RSE inventory[28] (see Supplementary Information for additional discussion on factors controlling RSE accumulation).

The U isotope values provide an independent confirmation of highly oxygenated oceans—as noted above they are the most positive shale δ^{238}U values measured to date (Figure 2), requiring both high seawater δ^{238}U values (likely comparable to the modern value of ~−0.4‰) and a near full expression of the equilibrium ~1.2‰ fractionation during U reduction. High seawater values only develop when oxic U burial is a major U burial flux in well-oxygenated oceans[36]. In addition, a significant positive U isotope fractionation ($\gg$0.6‰) strongly suggests U reduction in the water column instead of within the sediment pile[31]. Uranium reduction rates appear to scale with sulphate (or iron) reduction rates[37]—providing a link between amounts of organic matter loading in a marine system and the isotope fractionation that occurs during U burial. For reference, there is limited water column sulphate reduction in the modern Black Sea and Cariaco Basin because of low rates of productivity and maximum sediment δ^{238}U is only ~0.8‰ and ~0.6‰ higher than seawater, respectively[36]. In contrast, high productivity in the ZF is consistent with the anomalous organic carbon enrichments. Therefore, the strongly positive U isotope values in the ZF, along with the RSE enrichments, are most readily explained by invoking both globally well-oxygenated oceans and markedly elevated rates of local primary productivity, the latter of which would tend to enhance the expression of isotope effects associated with U reduction.

Conflicting views on oxygenation during ZF deposition

Our interpretation that the ZF records well-oxygenated ocean conditions is ostensibly in conflict with previous interpretations derived from C, S, and Mo isotope records proposed to reflect global deoxygenation. However, much of this data can plausibly be explained through local rather than global processes. First, Kump *et al.*[38] postulated a post-LJE global negative $\delta^{13}C$ excursion based on depleted $\delta^{13}C$ in ZF carbonates. This was interpreted to result from the widespread oxidation of organic-rich shales, which would have favoured suppressed, rather than elevated, O_2 levels. However, negative $\delta^{13}C$ in the ZF has subsequently been reinterpreted to reflect basin-wide methanotrophy and secondary overprinting of carbonate rocks[39]. Second, Scott *et al.*[5] argued that highly ^{34}S-enriched pyrites in the upper ZF reflect a global collapse of the marine sulphate reservoir due to deoxygenation. In contrast, Paiste *et al.*[40] explained the same trends through basin-specific processes involving quantitative uptake of sulphate. Third, Asael *et al.*[41,42] inferred an ~0.7‰ seawater $\delta^{98/95}Mo$ value from two other cores in the upper ZF, identical to the average in the OnZaP section. Mn-oxides, which form in oxic waters, preferentially scavenge ^{95}Mo and drive seawater $\delta^{98/95}Mo$ to higher values. If one assumes a modern riverine input value of ~0.7‰ for the Paleoproterozoic[30], a seawater value of ~0.7‰ suggests limited Mn-oxide precipitation and, thus, little O_2 in the oceans. However, the sequestration of Mo in sediments commonly imparts a negative $\delta^{98/95}Mo$ fractionation, except in highly restricted euxinic basins where nearly all Mo is drawn down[30]. This highlights that the highest Mo isotope values of ~1.4‰ represent a minimum seawater $\delta^{98/95}Mo$ estimate (see Ref. 11 and Supplementary Information) and that the Mo isotope data does not necessarily preclude widespread oxic conditions.

Implications of oxygenated oceans at approximately 2000 Ma

RSE-replete conditions during the deposition of the ZF have important implications for Earth's global C and O cycles during the Paleoproterozoic. Tracking the evolution of Earth's redox history is also critical for understanding early eukaryote evolution. The late rise to prevalence of eukaryotes in the Neoproterozoic is thought to be linked to widespread anoxic and nutrient-poor conditions that favoured prokaryotic metabolisms[43]. Given the extent of ocean oxygenation and nutrient abundance inferred from the ZF[3,44], conditions favourable to eukaryotic diversification could have been present for much of the middle Paleoproterozoic. It is curious, then, that molecular clock analyses and microfossil evidence of eukaryote origin tend to converge after ~1900 Ma[45,46]. In the simplest sense this discrepancy supports the central importance of a unique endosymbiosis event for the emergence of eukaryotes, rather than removal or lessening of an environmental barrier.

The ZF is part of a well-recognized overall trend towards elevated RSE concentrations at ~2400–2000 Ma that has been linked to well-oxygenated oceanic–atmospheric conditions[8–10]. Surprisingly, our ZF data extend this trend past the termination of the LJE. Furthermore, the extreme RSE enrichments hint that, instead of being in decline, atmospheric O_2 abundance could still have been high perhaps several tens of Myrs after the canonical end of the LJE[16]. In the modern, well-oxygenated world, the geologic O_2 response time is on the order of ~2 Myrs[47], whereas the residence times of Mo, U, and Re in the oceans are ~440, ~400, and ~780 kyrs, respectively[25,27]. Therefore, if the LJE decline is linked to a decrease in O_2 production as the result of diminishing C_{org} burial by the end of the LJE, then O_2 would be expected to be significantly attenuated by this time. Instead, our data suggest the opposite.

Our observations provide empirical evidence for models (e.g., Ref. 13) that decouple the strongly positive carbonate carbon isotope values of the LJE from enhanced organic carbon burial. Further, given the likelihood that highly oxidized conditions continued up to ~2.0 Ga, this highlights the importance of exploring alternative interpretations of the carbon isotope record and the need for refined chemostratigraphic and geochronological studies focused on this key interval of Earth's history.

References

1. Karhu, J. A. & Holland, H. D. Carbon isotopes and the rise of atmospheric oxygen. *Geology* **24**, 867–870 (1996).
2. Martin, A. P., Condon, D. J., Prave, A. R. & Lepland, A. A review of temporal constraints for the Palaeoproterozoic large, positive carbonate carbon isotope excursion (the Lomagundi–Jatuli Event). *Earth-Sci. Rev.* **127**, 242–261 (2013).
3. Bekker, A. & Holland, H. D. Oxygen overshoot and recovery during the early Paleoproterozoic. *Earth Planet. Sci. Lett.* **317–318**, 295–304 (2012).
4. Planavsky, N. J., Bekker, A., Hofmann, A., Owens, J. D. & Lyons, T. W. Sulfur record of rising and falling marine oxygen and sulfate levels during the Lomagundi event. *Proc. Natl. Acad. Sci. U.S.A.* **109**, 18300–18305 (2012).
5. Scott, C. *et al.* Pyrite multiple-sulfur isotope evidence for rapid expansion and contraction of the early Paleoproterozoic seawater sulfate reservoir. *Earth Planet. Sci. Lett.* **389**, 95–104 (2014).
6. Blättler, C. L. *et al.* Two-billion-year-old evaporites capture Earth's great oxidation. *Science* **360**, 320–323 (2018).

7. Konhauser, K. O. *et al.* Aerobic bacterial pyrite oxidation and acid rock drainage during the Great Oxidation Event. *Nature* **478**, 369–373 (2011).
8. Partin, C. A. *et al.* Large-scale fluctuations in Precambrian atmospheric and oceanic oxygen levels from the record of U in shales. *Earth Planet. Sci. Lett.* **369–370**, 284–293 (2013).
9. Kipp, M. A., Stüeken, E. E., Bekker, A. & Buick, R. Selenium isotopes record extensive marine suboxia during the Great Oxidation Event. *Proc. Natl. Acad. Sci. U.S.A.* **114**, 875–880 (2017).
10. Sheen, A. I. *et al.* A model for the oceanic mass balance of rhenium and implications for the extent of Proterozoic ocean anoxia. *Geochim. Cosmochim. Acta* **227**, 75–95 (2018).
11. Canfield, D. E. *et al.* Oxygen dynamics in the aftermath of the Great Oxidation of Earth's atmosphere. *Proc. Natl. Acad. Sci. U.S.A.* **110**, 16736–16741 (2013).
12. Bachan, A. & Kump, L. R. The rise of oxygen and siderite oxidation during the Lomagundi Event. *Proc. Natl. Acad. Sci. U.S.A.* **112**, 6562–6567 (2015).
13. Miyazaki, Y., Planavsky, N., Bolton, E. W. & Reinhard, C. T. Making sense of massive carbon isotope excursions with an inverse carbon cycle model. *J. Geophys. Res. Biogeosci.* **123**, 2485–2496 (2018).
14. Melezhik, V. A., Fallick, A. E., Medvedev, P. V. & Makarikhin, V. V. Extreme $^{13}C_{carb}$ enrichment in ca. 2.0 Ga magnesite–stromatolite–dolomite–`red beds' association in a global context: a case for the world-wide signal enhanced by a local environment. *Earth-Sci. Rev.* **48**, 71–120 (1999).
15. Eguchi, J., Seales, J. & Dasgupta, R. Great Oxidation and Lomagundi events linked by deep cycling and enhanced degassing of carbon. *Nat. Geosci.* **13**, 71–76 (2020).
16. Martin, A. P. *et al.* Multiple Palaeoproterozoic carbon burial episodes and excursions. *Earth Planet. Sci. Lett.* **424**, 226–236 (2015).

17. Melezhik, V. A., Fallick, A. E., Brasier, A. T. & Lepland, A. Carbonate deposition in the Palaeoproterozoic Onega basin from Fennoscandia: a spotlight on the transition from the Lomagundi-Jatuli to Shunga events. *Earth-Sci. Rev.* **147**, 65–98 (2015).
18. Kreitsmann, T. *et al.* Hydrothermal dedolomitisation of carbonate rocks of the Paleoproterozoic Zaonega Formation, NW Russia — Implications for the preservation of primary C isotope signals. *Chem. Geol.* **512**, 43–57 (2019).
19. Sadler, P. M. The influence of hiatuses on sediment accumulation rates. *GeoRes. Forum* **5**, 15–40 (1999).
20. Böning, P. *et al.* Geochemistry of Peruvian near-surface sediments. *Geochim. Cosmochim. Acta* **68**, 4429–4451 (2004).
21. Reinhard, C. T. *et al.* Proterozoic ocean redox and biogeochemical stasis. *Proc. Natl. Acad. Sci. U.S.A.* **110**, 5357–5362 (2013).
22. Wang, X. *et al.* A Mesoarchean shift in uranium isotope systematics. *Geochim. Cosmochim. Acta* **238**, 438–452 (2018).
23. Yang, S., Kendall, B., Lu, X., Zhang, F. & Zheng, W. Uranium isotope compositions of mid-Proterozoic black shales: Evidence for an episode of increased ocean oxygenation at 1.36Ga and evaluation of the effect of post-depositional hydrothermal fluid flow. *Precambrian Res.* **298**, 187–201 (2017).
24. Dunk, R. M., Mills, R. A. & Jenkins, W. J. A reevaluation of the oceanic uranium budget for the Holocene. *Chem. Geol.* **190**, 45–67 (2002).
25. Miller, C. A., Peucker-Ehrenbrink, B., Walker, B. D. & Marcantonio, F. Re-assessing the surface cycling of molybdenum and rhenium. *Geochim. Cosmochim. Acta* **75**, 7146–7179 (2011).

26. Crusius, J., Calvert, S., Pedersen, T. & Sage, D. Rhenium and molybdenum enrichments in sediments as indicators of oxic, suboxic and sulfidic conditions of deposition. *Earth Planet. Sci. Lett.* **145**, 65–78 (1996).
27. Anderson, R. F., Fleisher, M. Q. & LeHuray, A. P. Concentration, oxidation state, and particulate flux of uranium in the Black Sea. *Geochim. Cosmochim. Acta* **53**, 2215–2224 (1989).
28. Algeo, T. J. & Lyons, T. W. Mo–total organic carbon covariation in modern anoxic marine environments: Implications for analysis of paleoredox and paleohydrographic conditions. *Paleoceanography* **21**, PA1016 (2006).
29. Helz, G. R. *et al.* Mechanism of molybdenum removal from the sea and its concentration in black shales: EXAFS evidence. *Geochim. Cosmochim. Acta* **60**, 3631–3642 (1996).
30. Kendall, B., Dahl, T. W. & Anbar, A. D. The stable isotope geochemistry of molybdenum. *Rev. Mineral. Geochem.* **82**, 683–732 (2017).
31. Andersen, M. B., Stirling, C. H. & Weyer, S. Uranium Isotope Fractionation. *Rev. Mineral. Geochem.* **82**, 799–850 (2017).
32. Dickson, A. J. A molybdenum-isotope perspective on Phanerozoic deoxygenation events. *Nat. Geosci.* **10**, 721–726 (2017).
33. Tribovillard, N., Algeo, T. J., Lyons, T. & Riboulleau, A. Trace metals as paleoredox and paleoproductivity proxies: An update. *Chem. Geol.* **232**, 12–32 (2006).
34. Och, L. M. & Shields-Zhou, G. A. The Neoproterozoic oxygenation event: Environmental perturbations and biogeochemical cycling. *Earth-Sci. Rev.* **110**, 26–57 (2012).
35. Föllmi, K. B. *et al.* Phosphogenesis and organic-carbon preservation in the Miocene Monterey Formation at Naples Beach, California - The Monterey hypothesis revisited. *Bull. Geol. Soc. Am.* **117**, 589–619 (2005).

36. Andersen, M. B. *et al.* A modern framework for the interpretation of $^{238}U/^{235}U$ in studies of ancient ocean redox. *Earth Planet. Sci. Lett.* **400**, 184–194 (2014).

37. Barnes, C. E. & Cochran, J. K. Uranium geochemistry in estuarine sediments: Controls on removal and release processes. *Geochim. Cosmochim. Acta* **57**, 555–569 (1993).

38. Kump, L. R. *et al.* Isotopic evidence for massive oxidation of organic matter following the Great Oxidation Event. *Science* **334**, 1694–1696 (2011).

39. Qu, Y., Črne, A. E., Lepland, A. & van Zuilen, M. A. Methanotrophy in a Paleoproterozoic oil field ecosystem, Zaonega Formation, Karelia, Russia. *Geobiology* **10**, 467–78 (2012).

40. Paiste, K. *et al.* Multiple sulphur isotope records tracking basinal and global processes in the 1.98 Ga Zaonega Formation, NW Russia. *Chem. Geol.* **499**, 151–164 (2018).

41. Asael, D. *et al.* Coupled molybdenum, iron and uranium stable isotopes as oceanic paleoredox proxies during the Paleoproterozoic Shunga Event. *Chem. Geol.* **362**, 193–210 (2013).

42. Asael, D., Rouxel, O., Poulton, S. W., Lyons, T. W. & Bekker, A. Molybdenum record from black shales indicates oscillating atmospheric oxygen levels in the early Paleoproterozoic. *Am. J. Sci.* **318**, 275–299 (2018).

43. Brocks, J. J. *et al.* The rise of algae in Cryogenian oceans and the emergence of animals. *Nature* **548**, 578–581 (2017).

44. Lepland, A. *et al.* Potential influence of sulphur bacteria on Palaeoproterozoic phosphogenesis. *Nat. Geosci.* **7**, 20–24 (2014).

45. Parfrey, L. W., Lahr, D. J. G., Knoll, A. H. & Katz, L. A. Estimating the timing of early eukaryotic diversification with multigene molecular clocks. *Proc. Natl. Acad. Sci. U.S.A.* **108**, 13624–13629 (2011).

46. Betts, H. C. *et al.* Integrated genomic and fossil evidence illuminates life's early evolution and eukaryote origin. *Nat. Ecol. Evol.* **2**, 1556 (2018).

47. Kasting, J. F. & Canfield, D. E. The Global Oxygen Cycle. in *Fundamentals of Geobiology* (eds. Knoll, A. H., Canfield, D. E. & Konhauser, K. O.) 93–104 (John Wiley & Sons, Chichester, 2012).

48. McLennan, S. M. Relationships between the trace element composition of sedimentary rocks and upper continental crust: Trace element composition and upper continental crust. *Geochem. Geophys. Geosyst.* **2**, 1021 (2001).

49. Karhu, J. A. Carbon isotopes. in *Encyclopedia of Geochemistry* (eds. Marshall, C. P. & Fairbridge, R. W.) 67–73 (Kluwer Academic Publishers, Boston, 1999).

50. Robbins, L. J. *et al.* Trace elements at the intersection of marine biological and geochemical evolution. *Earth-Sci. Rev.* **163**, 323–348 (2016).

Corresponding author

Correspondence to Kaarel Mänd.

Acknowledgements

E. Ponzevera, A. De Prunelé, M.L. Rouget, K. von Gunten, and F. Zhang are thanked for help with trace element and isotope analyses. KM, KK, AL, TK, PP and KP were supported by the Estonian Research Council grant PRG447. KM was further supported by the Ministry of Education and Research of Estonia mobility grant within Archimedes Foundation's The Kristjan Jaak Scholarship program "Doctoral Study Abroad"; KP was supported by the Research Council of Norway through its Centres of Excellence funding scheme grant No. 223259; NJP and CTR

acknowledge support from the NASA Alternative Earths Astrobiology Institute; KOK was supported by the Natural Sciences and Engineering Research Council of Canada Discovery grant (RGPIN-165831).

Author contributions

AL, KK, KOK, SVL, and KM conceived the study. KM, KP, TK, AER, KK, and AL conducted field studies and organized the sample acquisition. KP, TK, AER, KK, and AL provided the geological and sedimentary background. KP provided additional TOC data. KM, LJR, SVL, MT, PP, CTR, KL, AV, and KOK measured and interpreted the trace metal abundance data. MT, SVL, and KM analyzed and interpreted the Mo isotope data. NJP, LJR, and KM analyzed and interpreted the U isotope data. SVL, TK, PP and KK analyzed and interpreted *in-situ* trace metal abundance. KM wrote the manuscript with input from all of the co-authors.

Competing interests

The authors declare no competing interests.

Figure captions

Figure 1: Lithology and geochemistry of the Zaonega Formation. Total organic carbon (TOC) and redox sensitive metal (RSE) profiles (errors contained within symbols), and Mo and U isotope ratios ($\delta^{98/95}$Mo and δ^{238}U, error bars are 2×SE) are shown for the OnZaP and OPH sections. Vertical dashed lines are average crustal values[30,31,48] and the dotted horizontal line is the phosphorous-rich mudstone–dolostone contact used for intra-basinal correlation (see Methods

and Supplementary Information). Boxplots below the Mo and U isotope plots represent the distribution of previously published ZF data from lower in the succession (see Supplementary Information)[41,42]. Gray horizontal bands are partly silicified and calcified intervals due to fluid alteration[40]. While these imply the presence of secondary fluids that could have mobilized RSE, microscale RSE distribution confirms the primary nature of the RSE enrichments (see Supplementary Information).

Figure 2: Secular trends in redox sensitive element concentrations from anoxic shales. Zaonega Formation data (plus and circle symbols) are plotted on compilations from literature (X symbols). (a) Changes in $\delta^{13}C_{carb}$ ratio through time, modified from Ref. 49. (b) Molybdenum concentrations from Ref. 50. (c) Uranium concentrations from Ref. 8. (d) Uranium isotope ratios from Refs. 22 and 23. (e) Rhenium concentrations from Ref. 10. Concentration errors are within symbols; for $\delta^{238}U$ and age errors, refer to Fig. 1, Supplementary Information, and compilation data sources.

Methods

Materials

The material for this study comes from drill cores in the Onega Basin that intersect the ZF—a relatively well-preserved 1500 m-thick succession of organic-rich mudstones and carbonates, interlayered and intersected with igneous units including lavas, tuffs, and sills (see Supplementary Information for a detailed geological setting)[51]. The 60 m long cores OnZaP-1 and OnZaP-3 were drilled 500 m apart in the northeastern part of the Onega Basin near Shunga village, close to drill core FAR-DEEP 13A[40]. The OnZaP-1 and OnZaP-3 cores are partly

overlapping and combined provide a 102 m thick OnZaP section. The 3500 m long OPH core that intersects the entire supracrustal succession of the Onega Basin was drilled ~60 km to the south. Paiste *et al.*[40,52] correlated the upper ZF OnZaP and OPH sections based on C isotopes, trace metal enrichments, P concentrations, and a distinct massive P-rich dolomite unit that occurs throughout the Onega Basin.

The lithology of this section is characterized by alternating dolomite to calcite-rich carbonates and exceptionally organic-rich mudstones that are intersected by silica or pyrobitumen veins (Figure 1). In the OnZaP section, the interval from the bottom of the section to 53 m depth is dominated by highly organic-rich mudstones with relatively few carbonate beds; the 53–33 m interval is mostly dolostone and contains a distinctive dolomite unit; and the 33–1.7 m interval consists of grey mudstones and marly carbonate beds[40]. Two sets of samples from the OnZaP section were analyzed in this study. Set MSP0001 consists of 135 samples that were taken at roughly 1 m intervals and is identical to that used in Paiste *et al.*[40]. Set MSP0010 contains 79 samples that more specifically targeted RSE and organic-rich intervals. A set of 89 samples were analyzed from the 1060–1230 m interval of the OPH core that is roughly equivalent to the OnZaP section.

Elemental concentrations

Total organic carbon content of the MSP0001 and OPH samples were adapted from Paiste *et al.*[40] and were measured from powdered aliquots using a LECO SC-444 analyzer at the Geological Survey of Norway (NGU), Trondheim, Norway. Detection limit was 0.1 wt.% and precision better than 10%. For the MSP0010 set, TOC was measured at the Pôle Spectrométrie Océan, European Institute for Marine Studies (IUEM), Brest, France. Dried and powdered samples were combusted

277 in ceramic beakers at 500 °C for 24h and loss of mass on ignition was determined. Repeat
278 measurements of 7 samples generally differed by <1 wt.%.

279 Major and trace element compositions of MSP0001 samples were determined at Acme Labs,
280 Bureau Veritas Commodities Canada Ltd. The samples were first pulverized and combusted to
281 remove organic carbon. For major elements, the sample was fused in $LiBO_2$ flux, then digested,
282 whereas minor elements were analyzed from full digests in HNO_3, $HClO_4$, and HF. Measurements
283 utilized inductively coupled plasma optical emission spectrometry (ICP-OES) or mass
284 spectrometry (ICP-MS). Average relative standard deviation was less than 5% for all elements.
285 MSP0010 element composition was determined at IUEM. Samples were pulverized in a tungsten
286 carbide crusher and an agate mill, then combusted at 500 °C for 24h to remove organic carbon.
287 Major element concentrations were measured on a Jobin Yvon Horiba Ultima 2 ICP-OES after
288 digestion overnight at 80 °C in concentrated HF and HNO_3 and neutralization with boric acid to
289 retain Si. For trace element concentrations, digestion was performed in a class 1000 clean
290 laboratory, using distilled acids—samples mixed with concentrated HF and HNO_3 were heated to
291 80 °C overnight, then allowed to evaporate; this digestion was then repeated with concentrated
292 *aqua regia*, after which the sample was taken up in 6M HCl. Trace element concentrations were
293 measured on a Thermo Scientific Element 2 ICP-MS calibrated against commercial multi-element
294 standards and digested geostandards (e.g., BHVO-2). OPH major and trace elements were
295 measured on a Philips PW 1480 X-ray fluorescence spectrometer (XRF) equipped with a Rh X-ray
296 tube at the Geological Survey of Norway. For major elements 0.6 g of ground and combusted
297 (1000 °C) sample was fused into a bead in a CLAISSE FLUXER-BIS together with 4.2 g of $Li_2B_4O_7$.
298 For trace elements 2.4 g of Hoechst wax was mixed with 9.6 g of sample in a Spex Mixer/Mill and
299 pressed into a pellet using a Herzog pelletizing press. Major element detection limits were 0.01%

(P_2O_5, CaO), 0.5% (SiO_2), 0.02% (Al_2O_3), or 0.02% (MgO) and precision (1σ) was typically ~2%. Detection limits for trace elements were ≤10 μg g^{-1}.

Samples with a ratio of $(CaO+MgO)/(SiO_2+Al_2O_3)$ > 0.2—approximating >20 wt.% carbonate content—were excluded when calculating Mo, U, and Re averages, since compilations of RSE in black shales generally only include shale samples[8,10,21]. An exception was made for samples with >5 wt.% TOC, since such sediments would have played a role in trace metal cycling regardless of their mineralogical composition.

Mo isotopes

Mo isotopes were measured from fully digested OnZaP MSP0010 samples that were purified via column chromatography according to Ref. 41. A ^{97}Mo–^{100}Mo double spike was employed[53] and the isotopes were measured on a Thermo Scientific Neptune multi-collector ICP-MS at IFREMER, Brest, France. Data is expressed relative to NIST SRM 3134 = 0.25‰[54]. Detailed methodology is provided in the Supplementary Information.

U Isotopes

Samples for U isotopes were sequentially digested in a mixture of 3 mL HNO_3 and 1 mL HF at 100 °C for 24 hours, then aqua regia at 95 °C for 24 hours. Following each digestion step the sample was evaporated to dryness. Sample residues were taken up in 5 mL of 3M HNO_3 at 70 °C. All sample preparation was performed in a Pico-trace clean lab at the Yale Metal Geochemistry Center. Uranium isotope values were measured on a Thermo Neptune Multi-collector ICP-MS following the method in Ref. 22 using the IRMM-3636 233/236 U double spike. Accuracy and precision were monitored with concentration matched CRM112, CRM129a, and Ricca

321 geostandards. Error was less than 0.15‰. Detailed methodology is provided in the
322 Supplementary Information.

323 Data availability

324 The novel ZF geochemical data presented here will be available in the PANGAEA data repository
325 under the title "Trace metal concentrations and isotope compositions from the ~2.0 Ga black
326 shales of the Zaonega Formation, NW-Russia (drill cores OnZaP, OPH)"[55].

327 Methods references

51. Melezhik, V. A., Fallick, A. E., Filippov, M. M. & Larsen, O. Karelian shungite—an indication of 2.0-Ga-old metamorphosed oil-shale and generation of petroleum: geology, lithology and geochemistry. *Earth-Sci. Rev.* **47**, 1–40 (1999).
52. Paiste, K. Reconstructing the Paleoproterozoic sulfur cycle: Insights from the multiple sulfur isotope record of the Zaonega Formation, Karelia, Russia. PhD thesis, Univ. Tromsø (2018).
53. Siebert, C., Nägler, T. F. & Kramers, J. D. Determination of molybdenum isotope fractionation by double-spike multicollector inductively coupled plasma mass spectrometry. *Geochem. Geophys. Geosyst.* **2**, 1032 (2001).
54. Nägler, T. F. *et al.* Proposal for an international molybdenum isotope measurement standard and data representation. *Geostand. Geoanal. Res.* **38**, 149–151 (2014).
55. Mänd, K. *et al.* Trace metal concentrations and isotope compositions from the ~2.0 Ga black shales of the Zaonega Formation, NW-Russia (drill cores OnZaP, OPH). PANGAEA [DOI number pending] (2020).

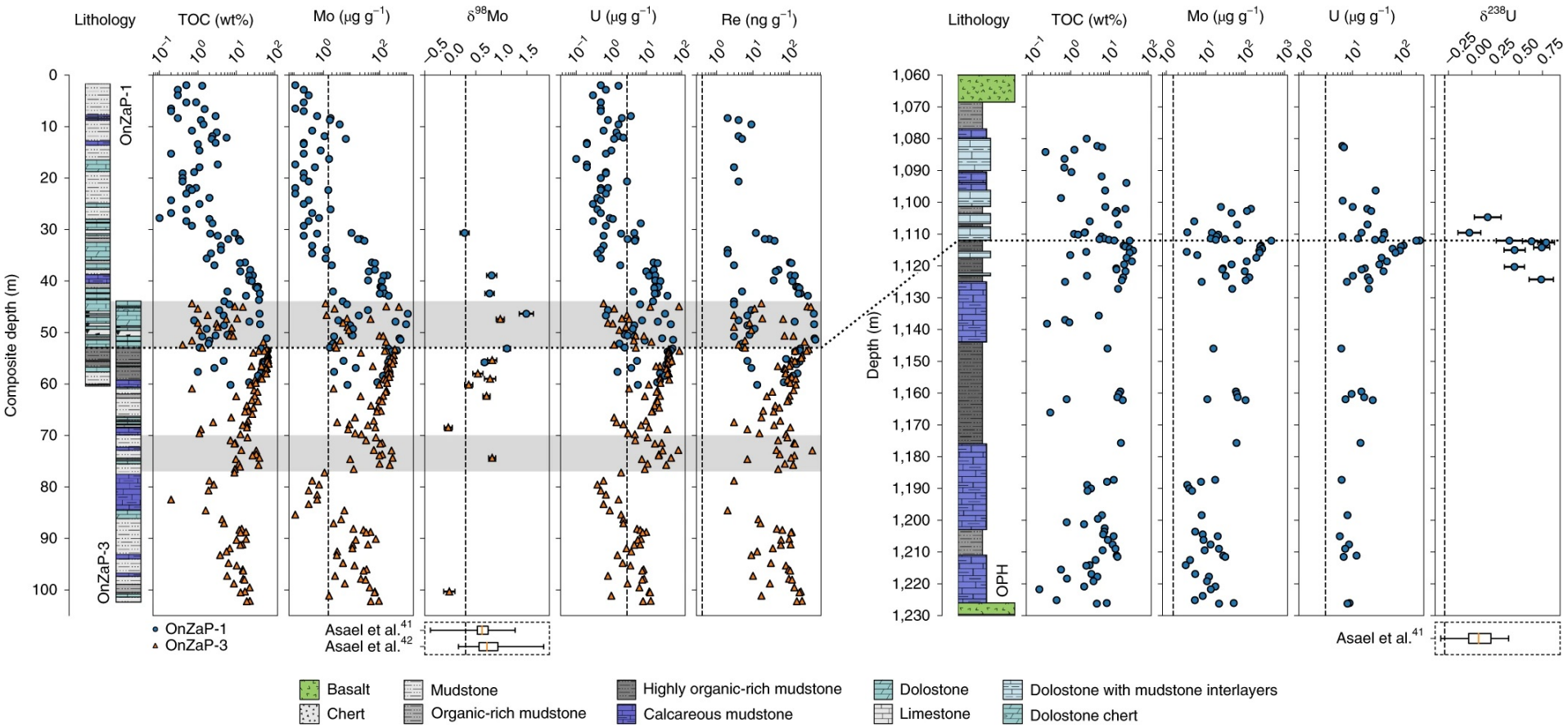
Lithology
TOC (wt%)
Mo (μg g−1)
δ98Mo
U (μg g−1)
Re (ng g−1)
Composite depth (m)
OnZaP-1
OnZaP-3
OnZaP-1
OnZaP-3
Asael et al.41
Asael et al.42
Depth (m)
OPH
δ238U
Asael et al.41
Basalt
Chert
Mudstone
Organic-rich mudstone
Highly organic-rich mudstone
Calcareous mudstone
Dolostone
Limestone
Dolostone with mudstone interlayers
Dolostone chert

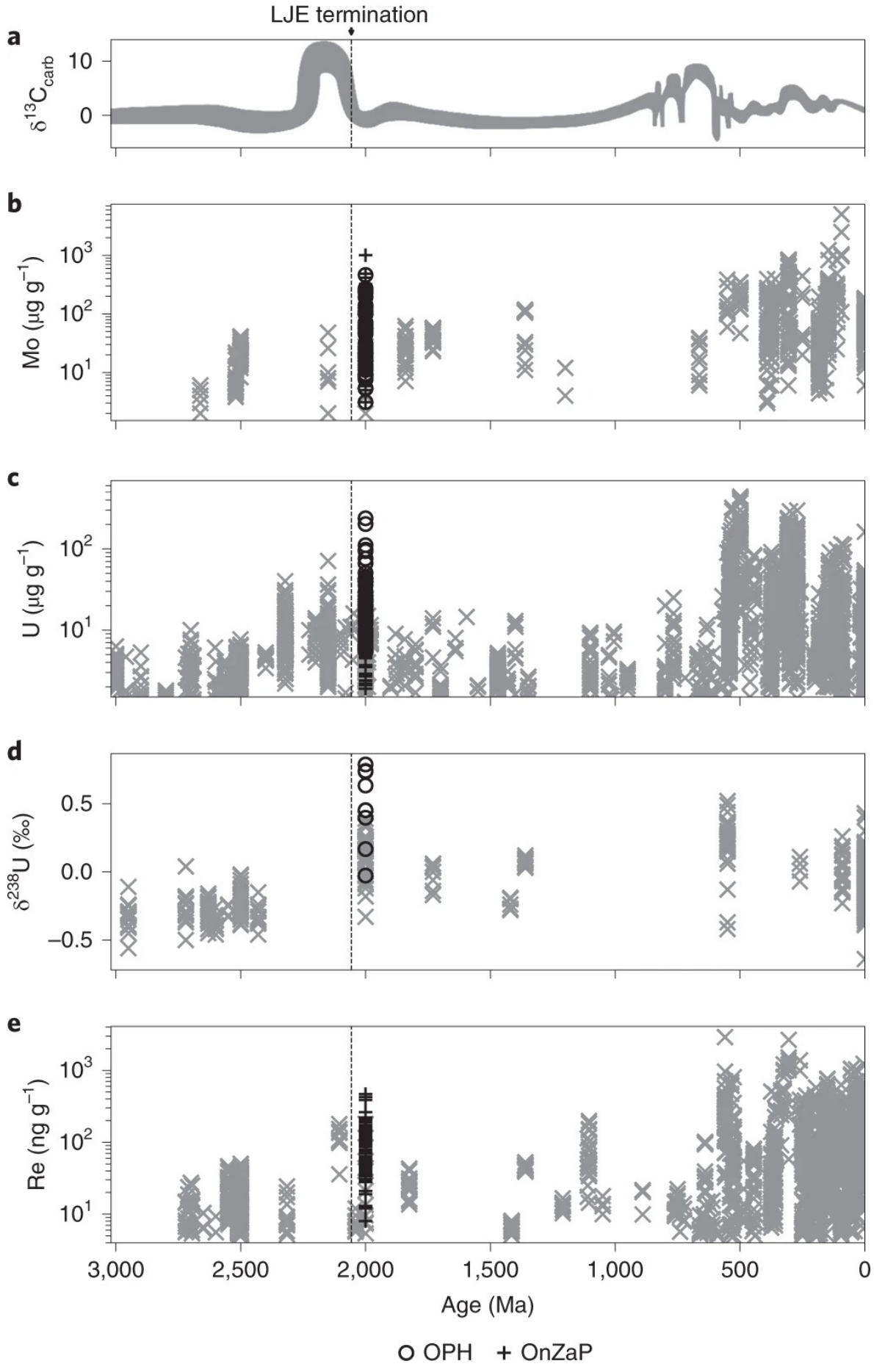
LJE termination
a
$\delta^{13}C_{carb}$
10
0
b
Mo (μg g^{-1})
10^3
10^2
10^1
c
U (μg g^{-1})
10^2
10^1
d
$\delta^{238}U$ (‰)
0.5
0.0
–0.5
e
Re (ng g^{-1})
10^3
10^2
10^1
3,000
2,500
2,000
1,500
1,000
500
0
Age (Ma)
OPH
OnZaP